JOURNAL OF PROPULSION AND POWER
Vol. 25, No. 3, May–June 2009

Performance Characteristics of an Annular Conical Aerospike Nozzle with Freestream Effect

S. B. Verma*
National Aerospace Laboratories, Bangalore 560 017, India

DOI: 10.2514/1.40302

An experimental investigation has been carried out to study the performance and base pressure characteristics of a Mach 2.0 annular conical aerospike nozzle with and without freestream flow. The effect of cowl length, plug length, and plug contour variation on the nozzle performance and base pressure characteristics is studied. It is observed that the overexpansion shock from the internal nozzle, overexpansion shock on the spike surface, and the expansion fan from the cowl lip of the internal nozzle dominate the overall flowfield development. The presence of freestream flow reduces the nozzle performance by approximately 4% relative to static conditions. Base pressure characteristics are observed to be strongly influenced by the movement of these shocks on the plug surface, and their subsequent interaction with the inner shear layer controls the base-wake closure. Relative to the conical plug configuration, the contoured plug shows considerably enhanced base pressure characteristics. Real-time pressure measurements on the spike reveal highly unsteady flow in the intermittent region of separation.

Nomenclature

$A_{\text{cowl exit}}$	=	annular area at the cowl exit, ms^{-1}
$C_f(i)$	=	thrust coefficient of an ideal nozzle
$C_f(x)$	=	estimated thrust coefficient, $F/A_t P_{\text{oj}}$
F	=	estimated thrust in the axial direction, N
f	=	fluctuation frequency, Hz
$G(f)$	=	power spectral density
h_t	=	height of the annular throat, mm
L	=	full length of the spike from the nozzle throat, mm
l	=	length of the cowl, mm
M_∞	=	freestream Mach number
P_a	=	ambient pressure, psi
P_b	=	plug base pressure, psi
P_c	=	stagnation chamber pressure, psi
$P_{\text{cowl exit}}$	=	pressure at the cowl exit, ms^{-1}
P_e	=	nozzle exit pressure, psi
P_{oj}	=	jet stagnation pressure, psi
P_w	=	local wall pressure on the spike surface, psi
$V_{\text{cowl exit}}$	=	velocity at the cowl exit, ms^{-1}
X	=	coordinate along the nozzle axis, mm
ϵ_i	=	area ratio of the internal nozzle
ϵ	=	area ratio of the aerospike nozzle

I. Introduction

CONVENTIONAL bell nozzles, due to their fixed geometry, suffer from reduced engine performance at low altitude due to overexpansion and at high altitude due to underexpansion; see Fig. 1a. Therefore, to achieve relatively better performance over the desired flight envelope, multistaging of the launch vehicle has been preferred to date. For first-stage application, the maximum geometric area ratio available is constrained by flow separation and the related side-load activity. For upper-stage applications, the maximum geometric area ratio is limited by the available integration volume [1]. But with a change in launcher stage design from the tandem to parallel configuration, the main stage engine is now expected to fulfill a wide range of operating conditions during the launcher's ascent [2]. Because these main-stage engines spend most of their flight time at high altitude, a designer prefers a high area-ratio

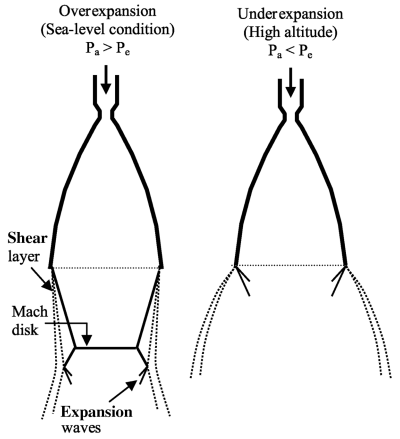

Fig. 1 Conventional bell nozzle: a) schematic of various flow conditions prevalent in a bell nozzle with a change in ambient pressure, and b) comparison of theoretical nozzles with conventional bell nozzles and aerospike nozzles [11].

Presented as Paper 5290 at the 44th AIAA/ASME/SAE Joint Propulsion Conference and Exhibit, Hartford, CT, 20–23 July 2008; received 7 August 2008; revision received 26 November 2008; accepted for publication 26 November 2008.

*Research Scientist, Experimental Aerodynamics Division, Council of Scientific & Industrial Research; sbverma@ead.cmmacs.ernet.in.

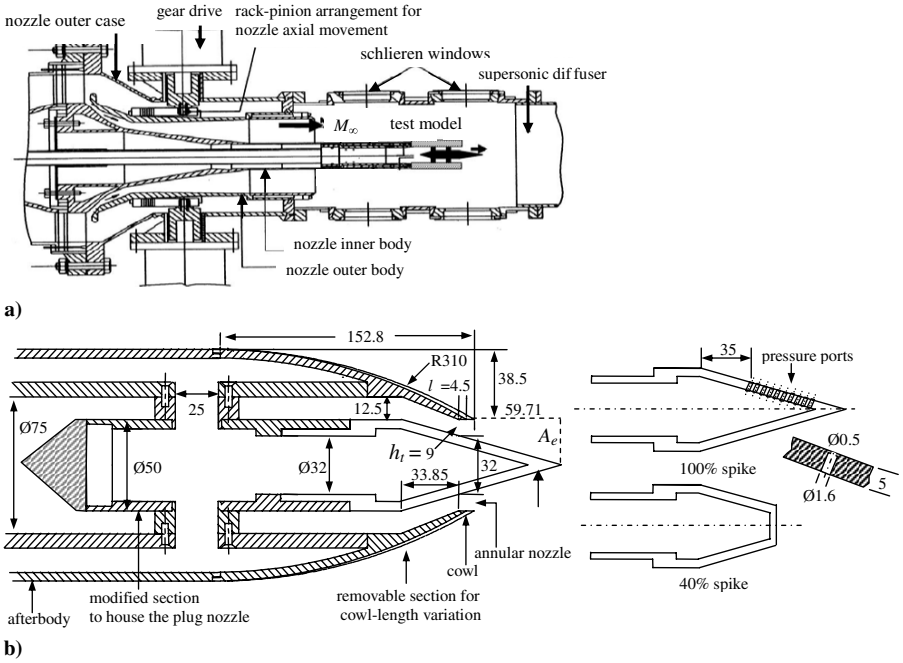

Fig. 2 Schematic showing a) the base flow facility at the National Aerospace Laboratories, and b) the plug mounting arrangements and cowl-length variation. All dimensions are in mm.

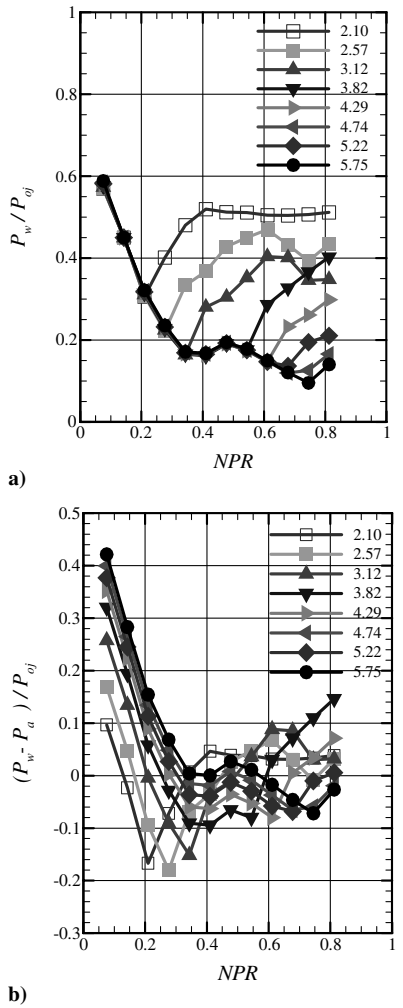

Fig. 3 Wall pressure measurements on the conical 100% length spike without the freestream flow; $l/h_t = 1.0$.

nozzle with high vacuum performance as the key requirement. But moderately large area-ratio nozzles operating at sea level produce separated exhaust flow, resulting in performance losses and high nozzle structural loads [3–6]. Therefore, an ideal nozzle would be one that continuously adjusts its contour, area ratio, and length to maximize thrust at each altitude, a concept known as altitude compensation. But variable area-ratio bell nozzles are mechanically complex and not cost effective for most applications [3].

Different types of nozzle concepts have been discussed and tested on the ground in the past [1,2,7–25]. These include the extendible nozzle [1] (widely used for upper-stage application) and the dual-bell nozzle [2] (still in the conceptual stage but a strong contender for the future Ariane vehicle) with single-step altitude adaptation capabilities, the annular/cluster plug nozzle [8,17–19] with continuous altitude adaptation for first- or upper-stage application, and the expansion-deflection thrust chamber [12] concept for the upper stage offering substantial decrease in integration volume without any moving parts. Other than the extendible nozzle, however, none of these concepts have reached hardware flight status. Recently, an annular aerospike nozzle has been tested for the first time in flight [26]. The linear concept of the annular/cluster plug nozzle is also foreseen as a strong contender for the propulsion system of reusable spacecraft [18,19].

The concept of aerospike nozzles was first reported in the 1960s [8–12] and 1970s [13–16], but has recently found renewed interest the world over as there is a need to increase the payload capacity of modern-day launch vehicles. The aerospike nozzle is, basically, a bell nozzle turned inside out that tends to maximize performance with altitude change. The outer wall of an aerospike (which serves as the inner wall of the bell) is always exposed to an ambient pressure, and so the external expansion allows continuous adaptation to ambient pressure during the entire flight trajectory. This eliminates overexpansion losses at altitudes below the nozzle design point. To get the highest benefit with this nozzle concept, the design pressure ratio and, thus, the geometrical area ratio should be chosen as high as possible, which could be realized with large launcher tail areas and/or high thrust chamber pressures. Figure 1b, reproduced from [11], shows a comparison of various nozzles. The ideal nozzle, indicated by the thick solid line, represents the maximum performance possible. It

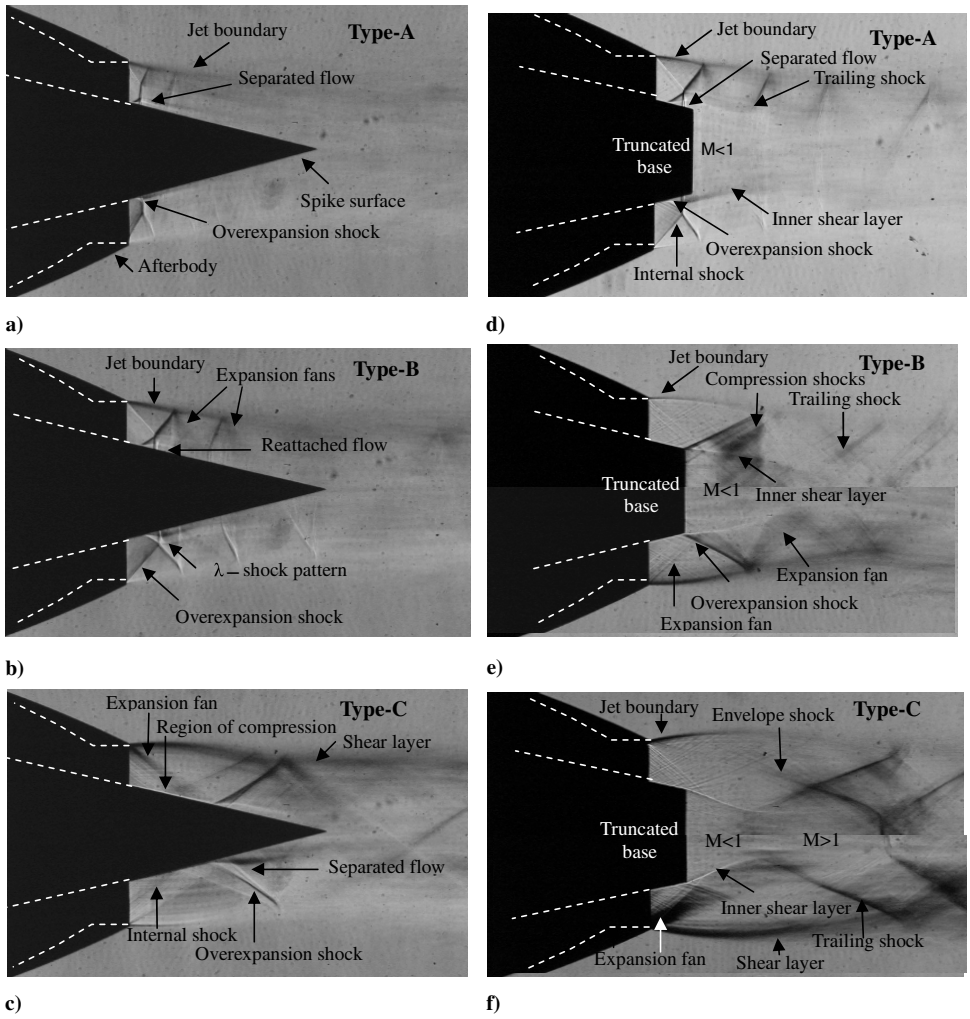

Fig. 4 Schlieren pictures with no freestream condition for the full-length spike: a) NPR = 2.1, b) NPR = 2.57, and c) NPR = 3.82. Schlieren pictures with no freestream condition for the 40% truncated spike: d) NPR = 2.57, e) NPR = 4.15, and f) NPR = 7.0.

can be clearly discerned that the aerospike shows the best performance at all altitudes. It has been further reported [17] that most of the thrust on the spike is generated over the first quarter, so that the remaining three-quarters can be truncated without much loss in total thrust. However, the thrust lost by removing some portion of the spike is compensated by the pressure acting on the base area of the truncated plug. Such a truncated plug nozzle configuration has the added advantages of a reduction in engine size and weight, which can then be used to increase the payload capacity of the launch vehicle, resulting in an overall gain in system performance. Altitude compensating effects still occur for such a truncated plug configuration although the flow structure downstream of the plug is significantly modified; hence, studies on plug nozzle configuration with and without freestream flow are of particular interest.

This paper reports the results of an experimental investigation performed on a 15 deg annular conical aerospike nozzle (design Mach number 2.0) with and without freestream flow. Earlier studies report that at low nozzle pressure ratio, or NPR (P_{0j}/P_a), the base pressure is nearly equal to ambient pressure and becomes constant at high NPR. The base pressure undergoes significant changes before and after this transition occurs, which need to be clearly understood for the prediction of base thrust characteristics. The main objective of the test campaign was, therefore, to correlate the variations in base pressure characteristics to changes in the plug flowfield through the effect of nozzle pressure ratio, percentage truncation, and cowl-length variation and study its implications on nozzle performance. A comparison of the nozzle performance for all test cases, with and without freestream, is made by evaluating the thrust generated on the spike/plug.

II. Experimental Setup and Procedure

A. Wind Tunnel and Test Conditions

Experiments were carried out in the 0.5 m base flow facility, a special purpose blowdown-type tunnel (Fig. 2a). Some of the special features of this tunnel are 1) an axisymmetric variable geometry nozzle, which can provide test Mach numbers in the range of 0.4 ± 0.01–3.5 ± 0.01 (and unit Reynolds numbers in the range of 10–$50 \pm 0.2 \times 10^6$ m^{-1}); 2) support of the models directly on the nozzle innerbody, thereby completely eliminating the support system interference; 3) fairly well-developed zero pressure gradient turbulent-boundary-layer characteristics on the afterbody; and 4) easier mounting and changing of the afterbody-nozzle models. The tunnel has been extensively calibrated, and the results indicate good mean flow uniformity and axisymmetry of the freestream and jet flow in the tunnel.

B. Model and Experimental Setup

The $M_j = 2.0 \pm 0.1$ conical (15 ± 0.03 deg half-angle) annular aerospike model was mounted on the central cylindrical inner body in such a way that different truncated sections of the spike/plug can be tested on the same cylindrical central body; see Fig. 2b. Up to 12 pressure points (with a pitch of 4 ± 0.1 mm) were fabricated along a single line on the full-length spike so as to investigate the flow in detail and to help evaluate the pressure thrust generated on the full-length spike. The exit nozzle radius, r_e, in this nozzle is fixed as 25 ± 0.1 mm. The annular gap at the throat section (h_t) is 9 ± 0.1 mm, and the length (L) of the spike is 59.7 ± 0.1 mm. The aerospike nozzle area is defined as the ratio of the area at spike end

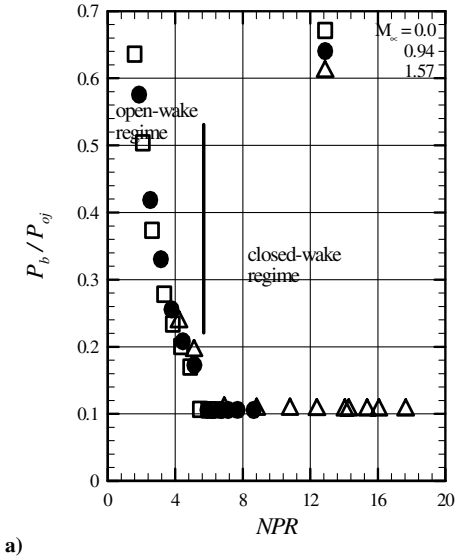

a)

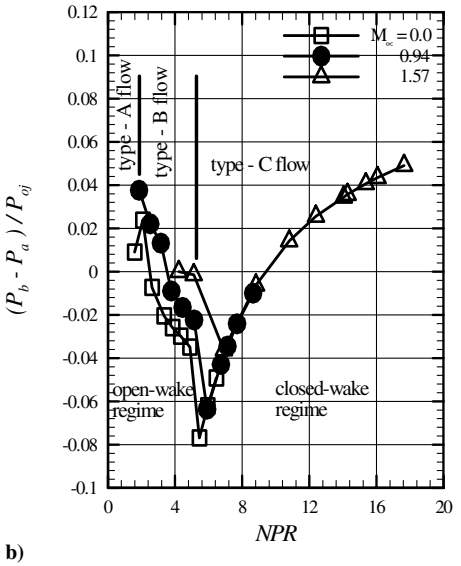

b)

Fig. 5 Base pressure variation with NPR showing the effect of freestream for a 40% truncation case; $l/h_t = 1.0$: a) P_b/P_{oj} vs NPR, and b) $(P_b - P_a)/P_{oj}$ vs NPR.

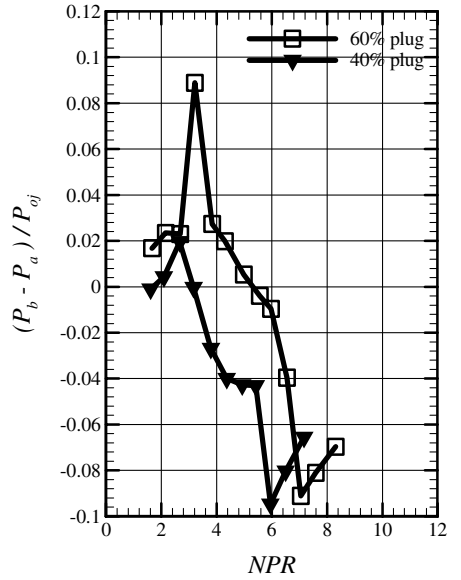

a)

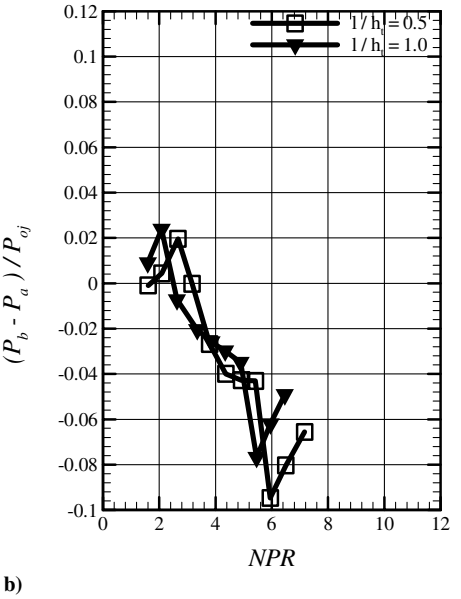

b)

Fig. 6 Comparison of base pressure variation for conical plug: a) effect of plug length, and b) effect of cowl length.

($r_e = 25 \pm 0.1$ mm) to the annular throat area. The length of the cowl, l (measured as the distance from throat section to the cowl lip), is varied between 4.5 ± 0.1 mm and 9.0 ± 0.1 mm, giving $l/h_t = 0.5 \pm 0.005$ and 1.0 ± 0.02 (resulting in $\epsilon_i = 1.1 \pm 0.01$ and $\epsilon_i = 1.19 \pm 0.01$, respectively). A 40% truncation of the full-length spike was also fabricated to study the effect of truncation on the overall nozzle performance. The truncated spike, however, had only five pressure ports for thrust evaluation. Two static pressure ports were included in the plug base region to acquire the base pressure and, hence, evaluate its contribution to the nozzle performance. Mean wall pressures were measured using Druck pressure scanners with a scan time of 8 s at each NPR. Simultaneous schlieren pictures were also taken at each NPR. A separate full-length conical spike model was fabricated to accommodate four Kulite (model XCE-062) pressure transducers to study the unsteady nature of separation shock oscillations. The afterbody contour was designed based on the recommendations given in [17]. The jet stagnation pressure, P_{oj}, was measured using a pitot tube ahead of the modified cylindrical section used to house the spike/plug, and the ambient pressure, P_a, was measured on the afterbody, 15 mm upstream of the cowl lip. The uncertainty in the measurement of P_{oj} is ± 0.2 psia, and that for P_w, P_b, and P_a is, respectively, ± 0.1 psia. In addition to static tests, a major part of the experiments were performed in the presence of freestream Mach numbers, M_∞, of 0.94 ± 0.02 and 1.57 ± 0.03. Thus, by varying the jet stagnation pressure P_{oj} to vary NPR, although the freestream Mach number is maintained, the local ambient pressure P_a decreases with each increase in P_{oj} (jet entrainment effect). Thus, the effect of the ambient pressure decrease in the presence of a freestream is easily simulated in such a facility and relates to real flight conditions.

III. Results and Discussion

A. Full-Length Spike

Figure 3a shows the streamwise mean wall pressure (P_w/P_{oj}) distribution on the full-length spike with a cowl length of 1.0 for different nozzle pressure ratios without freestream flow. For each test case, the NPR is held constant for 8 s. The point of incipient separation is marked by the first sudden increase in wall pressure in the pressure profiles. Higher NPR pushes the point of incipient separation downstream until the design NPR is reached, which shows no separation on the spike surface (full expansion). Examination of the wall pressure profiles shows a region of compression (seen as a hump) between X/L of 0.4–0.6. The wall

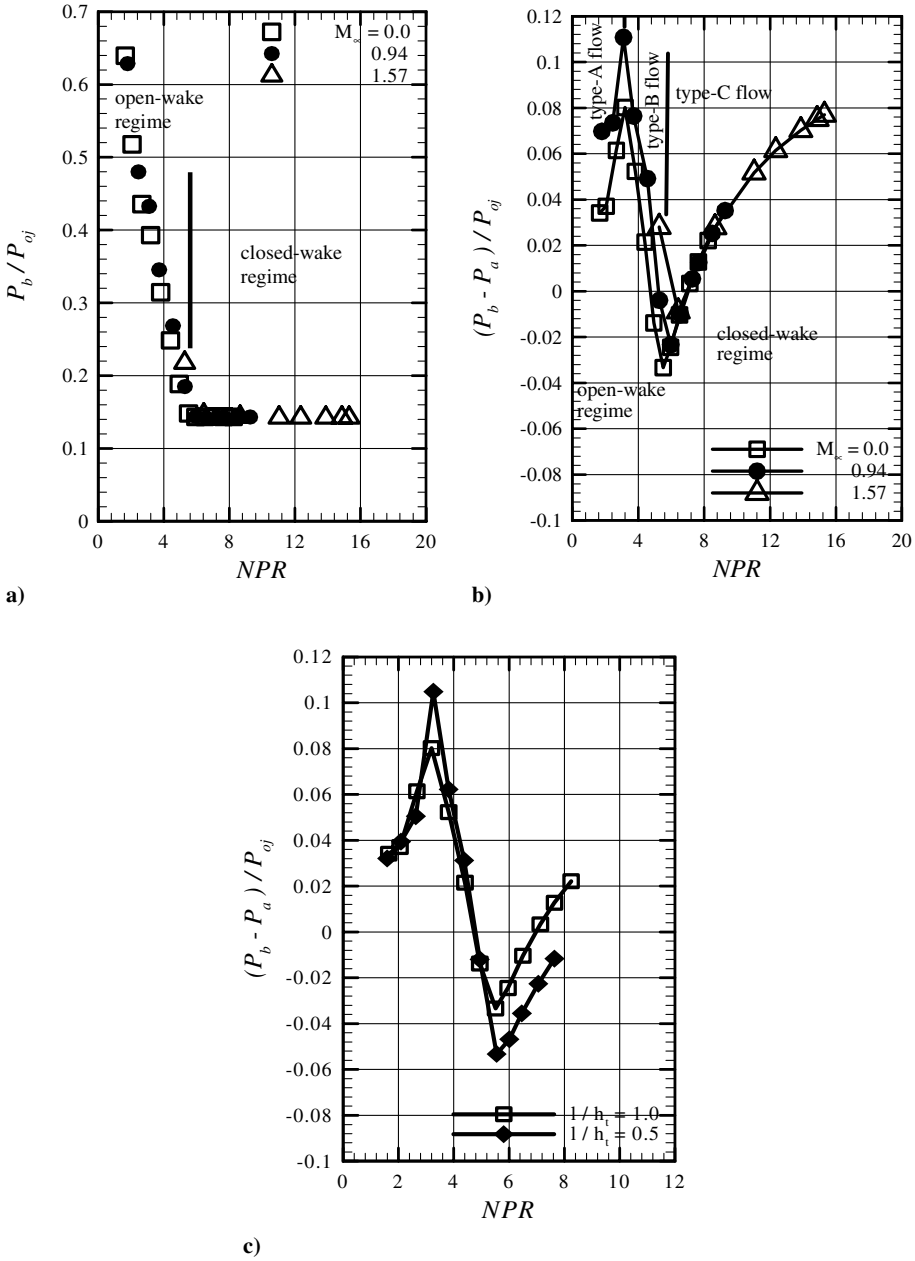

Fig. 7 Base pressure variation with NPR for a 45% contoured plug, $l/h_t = 1.0$: a) P_b/P_{oj} vs NPR, b) $(P_b - P_a)/P_{oj}$ vs NPR, and c) effect of cowl length.

pressures are also plotted with $(P_w - P_a)/P_{oj}$ along the Y axis; see Fig. 3b. According to this definition of nondimensional pressure (NDP) [22], an NDP > 0 indicates positive thrust and NDP < 0 indicates negative thrust.

Figures 4a–4c show schlieren pictures (with a horizontal knife edge) of the exhaust flowfield on the spike for three NPR. Basic flow characteristics that can be observed are the external jet boundary developing from the cowl exit, the internal nozzle overexpansion shock originating in the vicinity of the cowl lip, and the overexpansion shock formed on the spike surface. Increasing the NPR changes the angle of these shocks as the internal nozzle operates from the overexpanded to the underexpanded condition. This produces different flow conditions on the spike, which can be broadly classified into three types. At low NPR, the interaction between the overexpansion shock from the internal nozzle with the overexpansion shock on the spike results in a free shock separation condition; see Fig. 4a. This is designated as a type A flow, in which there is complete flow separation downstream of the point of incipient separation. At intermediate NPR between 2.57 and 3.12, a type B flow condition can be identified, as in Fig. 4b, in which the interaction between these overexpansion shocks cause flow reattachment (forming a λ-shock pattern) that increases the local wall pressure above ambient, as shown in Fig. 3b. A type C flow condition, seen in Fig. 4c, is produced when the internal nozzle starts to operate in an underexpanded condition. The expansion fan from the cowl lip overexpands the flow on the spike surface that results in the formation of an overexpansion/separation shock. At the same time, the internal shock originating from the throat of the internal nozzle impinges on the spike surface, forming a region of compression (seen as a pressure bump in Fig. 3a). At higher NPR, the expansion fan impinges further downstream, causing the overexpansion shock to move toward the end of the spike, and the pressure profiles gradually begin to resemble the profile at full expansion.

B. 40% Plug Nozzle

1. *Base Flow Characteristics (Conical Spike)*

Truncating the otherwise long spike modifies the exhaust flowfield considerably. Figures 4d–4f show the schlieren pictures of the flow for a 40% plug nozzle ($l/h_t = 1.0$) without freestream flow. To capture better flow details, the top half of the schlieren picture is

taken using a knife edge in horizontal position and the bottom half with a vertical knife edge. The accelerating flow on the plug expands around the corner, influencing the base pressure. An inner shear layer develops from the corner of the plug, dividing the plug flow from the base region; see Fig. 4e. Figures 5a and 5b show the base pressure characteristics as a function of NPR. The data in Fig. 5a largely show two major flow regimes, namely, the one during which the base pressure ratio (P_b/P_{oj}) continues to decrease sharply and the other that shows values with a constant base pressure ratio. These regimes have been identified [17–19,22] as "open wake" and "closed wake," respectively, based essentially on the influence of P_a (and, hence, the flow development on the plug and base region) on P_b.

Plotting $(P_b - P_a)/P_{oj}$ vs NPR [13], as in Fig. 5b, helps to better correlate the subtle changes in base pressure to the flowfield development on the plug nozzle, which are discussed. At low NPR (2.1), the overexpansion shock on the spike surface increases P_w to P_a downstream of separation whereas the reflected shock from the shock–shock interaction (between overexpansion shocks from the cowl lip and spike surface) intersects the free shear layer from the cowl lip and is reflected back to the separated shear layer as an expansion, upstream of the base region. This results in a positive base thrust. At NPR of 2.57, as in Fig. 4d, the change in angle of the overexpansion shocks from the internal nozzle modifies the shock–shock interaction in such a way that the reflected shock causes flow reattachment on the plug surface, which increases the base pressure. This flow condition is designated as type A. A short plug prevents further flow reattachment at higher NPR, and the overexpansion shock now sits exactly at the plug corner. The accelerated flow on the plug further expands around the corner, decreasing the base pressure. This is designated as a type B flow condition; see Fig. 4e. As the internal nozzle begins to operate in the underexpanded condition, the expansion fan from the cowl lip impinges on the inner shear layer, thereby strongly influencing the P_b so that now the base starts to deliver negative thrust. At NPR of about 5.5, the expansion fan from the cowl lip moves downstream of the sonic line and a sudden change in base flow characteristics is observed. At this point, P_b becomes insensitive to changes in P_a. The impingement of the expansion fan on the inner shear layer produces a strong trailing shock that is visible in Fig. 4f for NPR = 7.0. This is designated as a type C condition; see Fig. 4f. This sudden change in flow condition experienced for NPR $\geq$ 5.5 marks the transition from an open-wake regime to closed-wake regime; see Fig. 5. Up to this point, initially the overexpansion shock from the internal nozzle (and its subsequent reflection from the jet boundary) and later on the expansion fan from the cowl exit, containing information about P_a, directly affected P_b in the base region. But during the closed-wake regime, the base pressure ratio (P_b/P_{oj}) remains constant; see Fig. 5a. However, the nondimensional base pressure, $(P_b - P_a)/P_{oj}$, as in Fig. 5b, keeps on increasing primarily due to an increase in P_b with an increase in NPR. This causes the negative base thrust contribution to decrease gradually and, ultimately, at very high NPR, a positive thrust contribution occurs once again.

In the presence of freestream flow, the overall base pressure characteristics remain the same, except that now the transitions between different types of flow conditions occur at higher NPR (but lower P_{oj}) primarily due to the dominating effect of reduced P_a in these cases, which helps to improve the base thrust contribution significantly; see Fig. 5b. This is relevant to real flight conditions in which an early shift to the positive base thrust contribution (or in other words, less time spent under a negative base thrust contribution) is preferred to facilitate enhanced nozzle performance at low altitudes. Once under a closed-wake regime, the trend for $(P_b - P_a)/P_{oj}$ with and without the freestream condition is similar with increasing NPR.

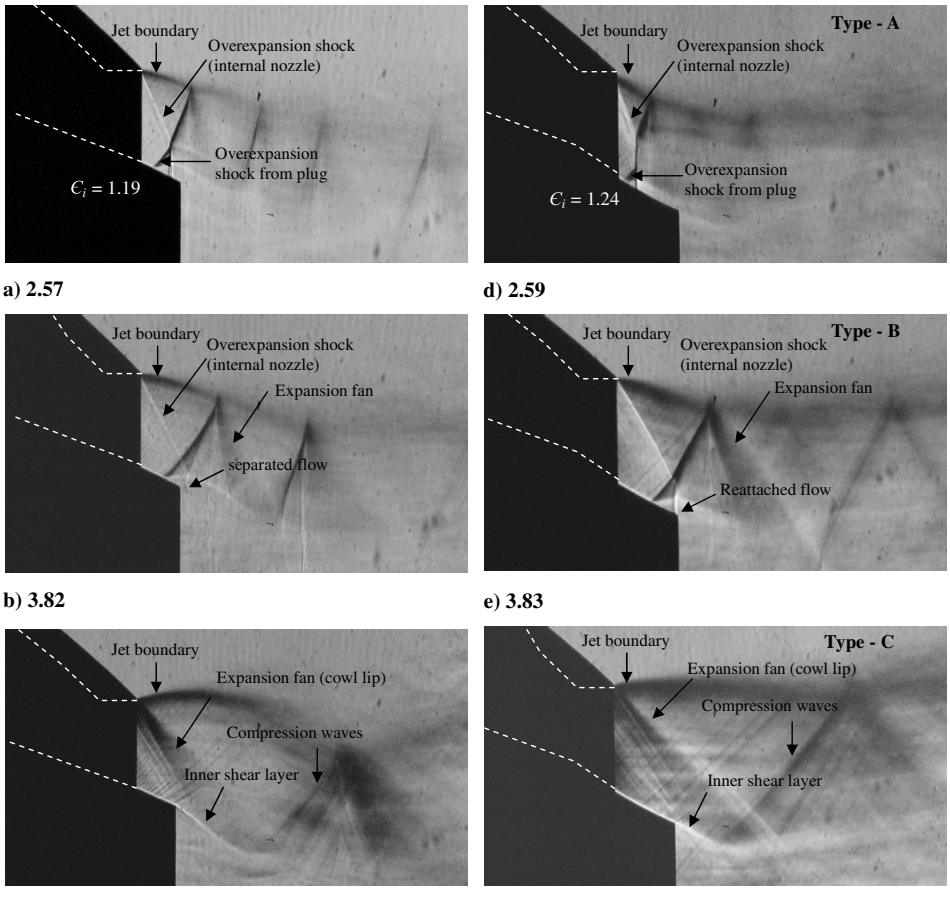

Fig. 8 Schlieren pictures with no freestream condition for the 40% conical spike: a) NPR = 2.57, b) NPR = 3.82, and c) NPR = 5.75. Schlieren pictures with no freestream condition for the 45% contoured spike: d) NPR = 2.59, e) NPR = 3.83, and f) NPR = 5.73.

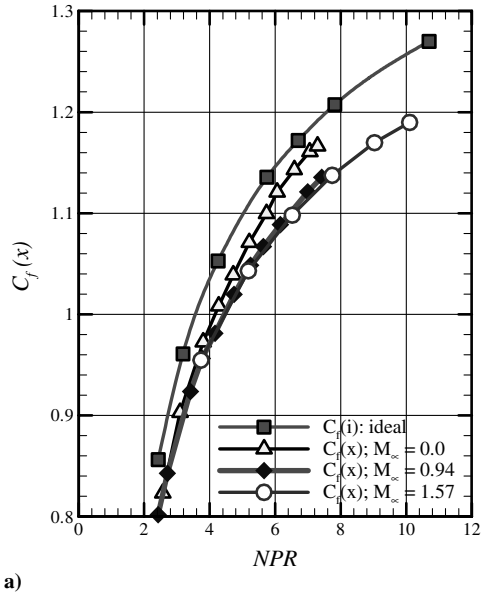

a)

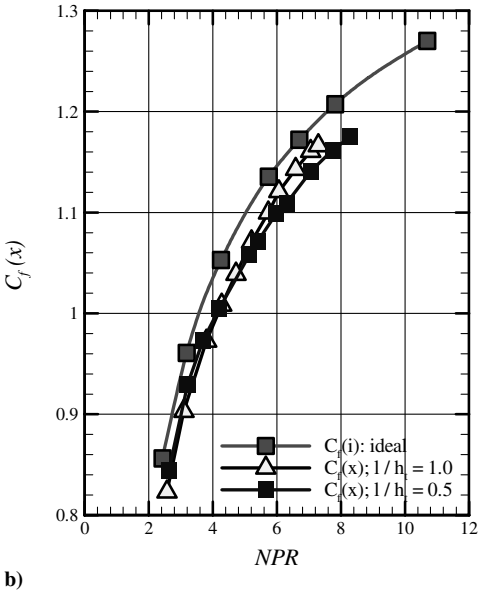

b)

Fig. 9 Performance comparison showing a) the effect of freestream, $l/h_t = 1.0$; and b) the effect of cowl-length variation; no freestream case.

2. Effect of Percentage Truncation and Cowl Length

Figure 6a shows the base flow characteristics as a function of percentage truncation without afterbody flow. The longer plug (60%) shows a higher base pressure ratio with flow transitions occurring at a higher NPR. This is because, on a longer plug, each flow regime continues to occur up to a higher NPR and so the wake closure also gets delayed. This is not desirable in real flight and so the use of shorter plugs (and, hence, early wake closure) is preferred. A longer cowl length also initiates a slight early wake closure, the benefits of which are somewhat similar to those achieved by using a shorter plug; see Fig. 6b.

C. Base Flow Characteristics (45% Contoured plug)

Because the base flow characteristics are very strongly influenced by the flow development on the plug surface, a contoured plug was fabricated using a minimum length nozzle (MLN) design procedure for a design Mach number of 2.0. All other model configurations were kept the same. Remarkable changes in the flow development and, hence, the base flow characteristics were observed. Figures 7a and 7b show the base pressure ratio variation for a 45% contoured plug nozzle. Relative to the conical plug configuration, as in Fig. 5b, contouring the plug is seen to enhance the base flow characteristics significantly. A much higher base pressure P_b is observed in each flow regime (which also reduces the NPR range contributing to negative base thrust) with minimal affect of freestream Mach number. Also in closed-wake regime, the base pressure is much higher for the contoured plug. The effect of cowl length is similar to that observed for the conical case; see Fig. 7c.

The reason for the observed behavior is that, for a given axial location (relative to conical plug), the area ratio of the internal nozzle for the contoured plug is higher ($\epsilon_i = 1.24$, although the total area ratio of the full-length aerospike nozzle is same). For a given NPR, therefore, flow separation on the contoured plug occurs relatively upstream to that occurring on the conical plug; see Figs. 8a and 8d. The internal nozzle is, therefore, more strongly overexpanded at similar NPR and remains in the overexpanded state for a larger NPR range. This helps increase P_b between NPR = 2.1 and 3.8, as in Fig. 7a, and this flow condition can be designated as type A. Once the overexpansion shock sits at the plug corner, the accelerated flow begins to reduce P_b as also observed for the conical plug (type B). But the process of wake closure is more strongly influenced by the movement of the expansion waves from the cowl lip impinging on the inner shear layer. Despite a longer plug (45%), the wake closure occurs at similar NPR as for the 40% conical plug (type C). This is because, for a contoured plug surface, the expansion waves from the cowl lip impinge on the inner shear layer at a relatively upstream distance (as in Figs. 8c and 8f, owing to a relatively lower level of underexpansion at similar NPR), and an early wake closure is initiated primarily due to a smaller base. The lower levels of underexpansion of the internal nozzle can be easily identified from the smaller bulge in the external jet boundary from the cowl lip for the contoured plug; see Figs. 8c and 8f. Thereafter, P_b increases, as also observed earlier, with an increase in NPR.

D. Performance Comparison

The thrust estimate for the aforementioned configurations was made using the following formula [27]:

$$F = [mV_{\text{cowl exit}} + (P_{\text{cowl exit}} - P_a)A_{\text{cowl exit}}] + \int (P_w - P_a)\cos 75\,\mathrm{d}A + (P_b - P_a)A_b$$

where dA is the elemental area on the spike surface. For the full-length spike, the last term is zero. An immediate effect of truncation is to produce a base pressure that once again contributes to both positive and negative thrust depending on the nozzle operating conditions, as seen in the preceding section.

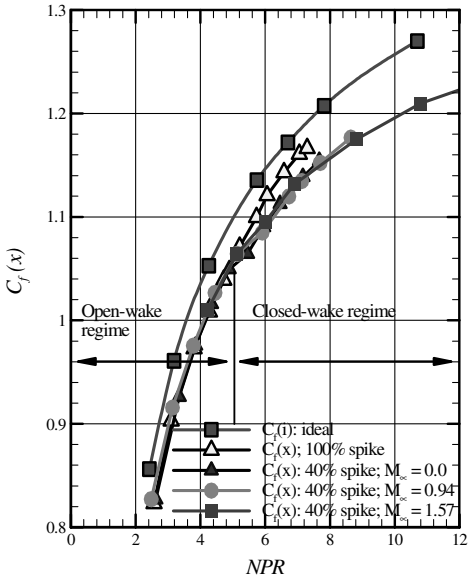

Fig. 10 Performance comparison showing the effect of freestream for the 40% truncation case; $l/h_t = 1.0$.

The coefficient of thrust of a nozzle is given by [27]

$$C_f(x) = F/(A_t P_{0j})$$

For an ideal nozzle ($P_e = P_a$), the optimum coefficient of thrust is given by

$$C_f(i) = \left\{ \frac{2k^2}{k-1} \left[\frac{2}{k+1} \right]^{\frac{k+1}{k-1}} \left[1 - \left[\frac{P_e}{P_{oj}} \right]^{\frac{k-1}{k}} \right] \right\}^{0.5}$$

It can be seen that, for the ideal case, the C_f value is dependent on gas property k and the pressure ratio across the nozzle and not on the type of nozzle.

Figure 9a shows a comparison of the C_f variation with NPR for no freestream condition and with cowl-length variation. The thrust in each case was estimated using the wall pressure distribution and integrating it over the conical surface area of the spike. The uncertainty in the evaluation of C_f is approximately $\pm 0.3\%$ at each test NPR. A comparison of the estimated C_f value for the test cases is also made with an ideal nozzle that changes its area ratio with a change in NPR. It can be seen that up to NPR 5 the two test cases show similar performance. Beyond NPR 5, the two curves begin to depart. Note that, for all test cases with NPR ≥ 6, flow separation does not occur on the plug and, therefore, relates the flow condition to main stage operation. The curve for the cowl length of 0.5 shows lower performance relative to the cowl length of 1.0. The difference is about 2% (of C_f) at NPR of 7.25. The probable reason is the higher contribution from the momentum term for $l/h_t = 1.0$ that overweighs the benefits of higher wall pressures on the spike for $l/h_t = 0.5$, especially at higher NPR.

The effect of freestream flow on the nozzle performance can be seen in Fig. 9b. The presence of freestream flow modifies the external jet boundary originating from the cowl lip significantly and, hence, the flow development on the spike if constant chamber pressure, P_{0j}, is maintained, which is relevant to real flight conditions. However, if similar NPR are to be maintained to evaluate and compare the thrust performance, then a lesser mass flow is required from the nozzle (due to lower P_{0j} required to maintain similar NPR as P_a decreases with an increasing M_∞) than for a nozzle with no freestream condition so that the momentum thrust contribution from the internal nozzle is relatively less with freestream flow. In either case, a reduction in net thrust results with an increasing NPR, as seen in Fig. 9b.

The truncated spike shows no change in the C_f value, with respect to that for the full-length spike, up to the point at which the flow undergoes a flow transition from an open-wake to close-wake regime; see Fig. 10. At this point, a sudden drop in the C_f value is observed, after which the C_f value once again increases with an increase in NPR. For different freestream conditions, a change in the C_f value trend is seen to occur at the NPR for which the base region closes for each test case. After this flow transition, a reduction in the C_f value is apparent between the truncated and full-length cases.

E. Spectral Analysis

Figures 11a and 11b show the schlieren picture of the type B flow condition (NPR = 3.1) on the full-length conical aerospike (without freestream) and the corresponding time history of a wall pressure signal in the intermittent separation region, respectively. The large-scale streamwise oscillatory motion or "flapping" of the shock wave can be easily identified; see Fig. 11b. The high level in wall pressure, P_2, is captured when the "foot" of the shock wave is upstream of the transducer, whereas level P_1 is captured when the shock wave translates downstream of the transducer location. Figures 11c and 11d show the power spectra of wall pressure fluctuations in the undisturbed boundary layer and in intermittent separation regions, respectively. A 1500 Hz peak in frequency can be seen in the region of separation, as in Fig. 11d, and downstream (not shown). The separation region also shows fluctuations in the 200–800 Hz range, suggesting highly unsteady flow conditions near separation shock.

IV. Conclusions

An experimental investigation has been carried out to study the performance characteristics of an annular conical aerospike nozzle (full length and 40% truncation). For no freestream condition, the performance of a full-length conical aerospike nozzle differs from the ideal case by about 3–4% (of C_f) at almost all NPR tested. A

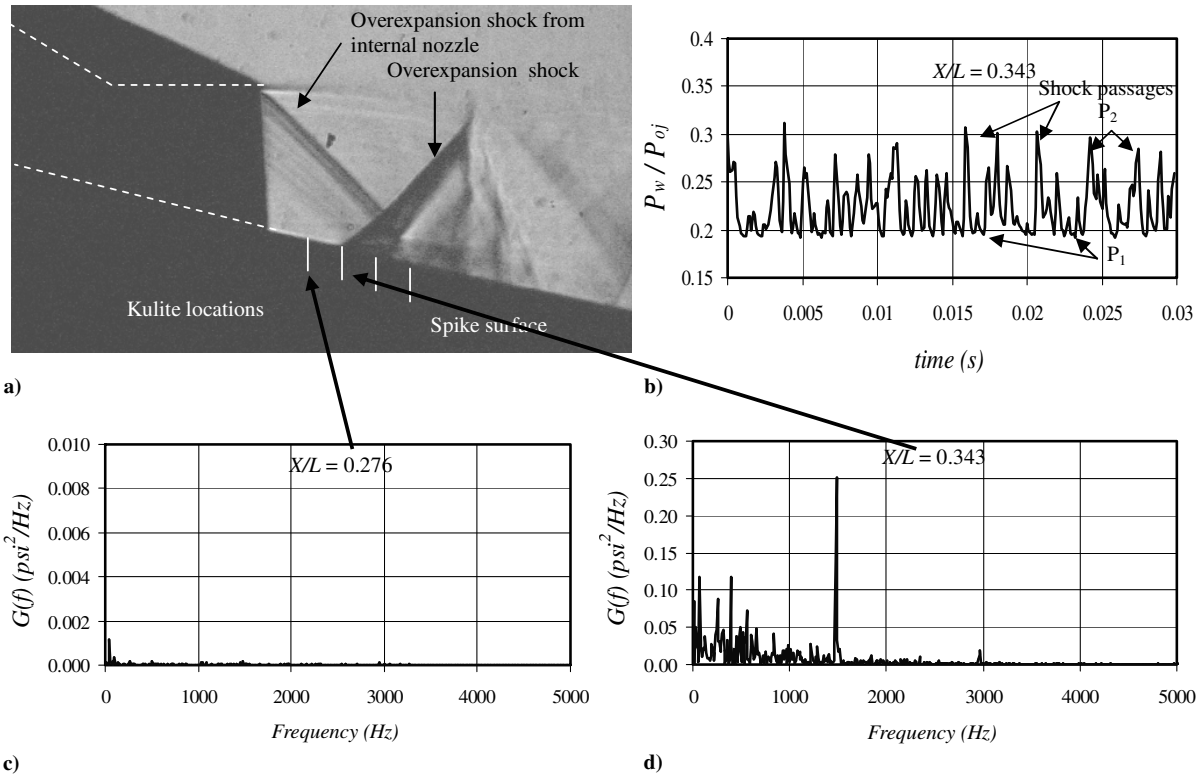

Fig. 11 Flow condition on a full-length conical aerospike nozzle: a) schlieren picture showing the shock structure details in a type B flow; b) time history of the wall pressure signals in an intermittent region of separation for NPR = 3.1, and c) and d) power spectral density in the separation region (first two locations).

reduction in cowl length to 0.5 further reduces the performance of the nozzle. In the presence of freestream conditions, the performance of the tested configurations further drops by 3% at the highest NPR.

Truncating the spike does not affect the nozzle performance except when the flow undergoes a transition from an open-wake to closed-wake regime. After this, although the C_f value continues to increase with an increase in NPR, a drop in performance relative to the full-length spike of about 3% is observed. Contouring the plug modifies the flowfield considerably, both on the plug and in the base-wake region, with significant improvement in overall base thrust contribution and minimum time spent under negative base thrust contribution.

Flow separation at low NPR indicates highly unsteady flow conditions on the full-length conical spike, which can result in undesirable lateral forces/side loads. To avoid this condition, it is preferred to use shorter plug nozzles so that they can switch to a closed-wake regime at lower altitudes. This can be further achieved by properly designing the plug contour and plug corner and by using an appropriate base-bleed system.

Acknowledgments

The author wishes to thank the Aeronautics Research and Development Board, India, for funding the project. The technical support of Rajshekhar Gowda during aerospike model design and fabrication and of A. Narayanswamy and V. Biju of the Base Flow facility at the National Aerospace Laboratories during the test campaigns is gratefully acknowledged. Many thanks to Francesco Nasuti of the University of Rome "La Sapienza," Tomita Takeo of the Japan Aerospace Exploration Agency, and Joesph Ruf of the NASA Marshall Space Flight Center for the useful discussions I had with them over e-mail during the planning and execution of this work.

References

[1] Hagemann, G., Immich, H., Nguyen, T. V., and Dumnov, G. E., "Advanced Rocket Nozzles," *Journal of Propulsion and Power*, Vol. 14, No. 5, Sept.–Oct. 1998, pp. 629–634.

[2] Stark, R., Boehm, C., Haidn, O. J., and Zimmermann, H., "Cold Flow Testing of Dual-Bell Nozzles in Altitude Simulation Chamber," *European Conference for Aerospace Sciences (EUCASS)*, 2006.

[3] Hagemann, G., Frey, M., and Koeschel, W., "Appearance of Restricted Shock Separation in Rocket Nozzles," *Journal of Propulsion and Power*, Vol. 18, No. 3, 2002, pp. 577–584. doi:10.2514/2.5971

[4] Oestlund, J., Damgaard, T., and Frey, M., "Side-Load Phenomena in Highly Overexpanded Rocket Nozzles," *Journal of Propulsion and Power*, Vol. 20, No. 4, 2004, pp. 695–704. doi:10.2514/1.3059

[5] Verma, S. B., Stark, R., and Haidn, O., "Relation Between Shock Unsteadiness and the Origin of Side-Loads in a Thrust Optimized Parabolic Rocket Nozzle," *Aerospace Science and Technology*, Vol. 10, No. 6, Sept. 2006.

[6] Verma, S. B., and Oskar, H., "Study on Restricted Shock Separation Phenomena in Rocket Nozzles," AIAA Paper 2006-1431, 2006.

[7] Manski, D., Hagemann, G., Frey, M., and Frenken, G., "Optimization of Dual Mode Rocket Engine Nozzles for SSTO Vehicles," IAF 98-S.3.08.

[8] Berman, K., and Crimp, F. W., Jr., "Performance of Plug-Type Rocket Exhaust Nozzles," *American Rocket Society Journal*, Jan. 1961, pp. 18–23.

[9] Rao, G. V. R., "Recent Developments in Rocket Nozzle Configurations," *American Rocket Society Journal*, Nov. 1961, p. 1488.

[10] Angelino, G., "Approximate Method for Plug Nozzle Design," *AIAA Journal*, Vol. 2, No. 10, Oct. 1964, pp. 1834–1835. doi:10.2514/3.2682

[11] Huzel, D. K., and Huang, D. H., "*Design of Liquid Propellant Rocket Engines*," NASA Science and Technical Information Office, Washington D.C., 1967, pp. 89–95.

[12] Wasko, R. A., "Performance of Annular Plug and Expansion-Deflection Nozzles Including External Flow Effects at Transonic Mach Numbers," NASA TN D-4462, April 1968.

[13] Humphreys, R. P., Thompson, H. D., and Hoffmann, J. D., "Design of Maximum Thrust Plug Nozzles for Fixed Inlet Geometry," *AIAA Journal*, Vol. 9, No. 8, Aug. 1971, pp. 1581–1587. doi:10.2514/3.49960

[14] Migdal, D., "Supersonic Annular Nozzles," *Journal of Spacecraft and Rockets*, Vol. 9, No. 1, Jan. 1972, pp. 3–6. doi:10.2514/3.61623

[15] Sule, W. P., and Mueller, T. J., "Annular Truncated Plug Nozzle Flowfield and Base Pressure Characteristics," *Journal of Spacecraft and Rockets*, Vol. 10, No. 11, 1973, pp. 689–695. doi:10.2514/3.61949

[16] Hall, C. R., Jr., and Mueller, T. J., "Exploratory Analysis of Nonuniform Plug Nozzle Flowfields," *Journal of Spacecraft and Rockets*, Vol. 9, No. 5, 1972, pp. 373–342. doi:10.2514/3.61684

[17] Ruf, J. H., and McConnaughey, P. K., "The Plume Physics Behind Aerospike Nozzle Altitude Compensation and Slipstream Effect," AIAA Paper 97-3217, 1997.

[18] Fick, M., and Schmucker, R. H., "Performance Aspects of Plug Cluster Nozzles," *Journal of Spacecraft and Rockets*, Vol. 33, No. 4, July–Aug. 1996, pp. 507–512. doi:10.2514/3.26792

[19] Rommel, T., Hagemann, G., Schley, C.-A., Kruelle, G., and Manski, D., "Plug Nozzle Flowfield Analysis," *Journal of Propulsion and Power*, Vol. 13, No. 5, Sept.–Oct. 1997.

[20] Hagemann, G., Immich, H., and Terhardt, M., "Flow Phenomena in Advanced Rocket Nozzles—The Plug Nozzle," AIAA Paper 98-3522, 1998.

[21] Dumnov, G. E., Nikulin, G. Z., and Ponomaryov, N. B., "Investigation of Advanced Nozzles for Rocket Engines," *Space Rocket Engines and Power Plants*, Vol. 4, No. 142, NIITP, 1993 (Published in Russian).

[22] Tomita, T., Tamura, H., and Takahashi, M., "An Experimental Evaluation of Plug Nozzle Flowfield," AIAA Paper 96-2632, 1996.

[23] Ito, T., Fujii, K., and Hayashi, A. K., "Computations of Axisymmetric Plug-Nozzle Flowfields: Flow Structures and Thrust Performance," *Journal of Propulsion and Power*, Vol. 18, No. 2, 2002, pp. 254–260. doi:10.2514/2.5964

[24] Yu, L., Zhengke, Z., Wuye, D., Jingsheng, Z., Shouen, Z., Xianchen, C., and Zhengpeng, Z., "Experimental and Numerical Studies on Aerospike Nozzles," AIAA Paper 99-2340, 1999.

[25] Wuye, D., Yu, L., and Xianchen, C., "Simulated Tests of Aerospike Nozzle and Data Acquisition System," *Journal of Propulsion Technology*, Vol. 21, No. 4, 2000, pp. 85–88.

[26] Norris, G.,"Solid Performance for Aerospike," *Flight International*, 27 April–3 May 2004, p. 28.

[27] Sutton, G. P., and Biblarz, O., *Rocket Propulsion Elements*, 7th ed., Wiley Interscience, New York, 2000.

K. Frendi
Associate Editor